

## Sample shape influence on the antiferroelectric phase transitions in dipolar systems subject to an external field

Yuriy V. Pereverzev, Oleg V. Prezhdo,\* and Larry R. Dalton

*Department of Chemistry, University of Washington, Seattle, Washington 98195-1700*

(Received 2 November 2001; published 8 January 2002)

A continuous change in the macroscopic shape of a sample from a needle through a sphere to a plate is shown to greatly affect phase transitions in Ising dipolar systems. The first- and second-order phase transition lines with critical and tricritical points appear, coexist, and disappear on the phase diagram with varying sample shape. The values of the shape-dependent depolarization factor corresponding to the changes in the phase diagram are identified.

DOI: 10.1103/PhysRevB.65.052104

PACS number(s): 64.70.-p, 42.70.Jk, 64.60.Kw, 77.80.-e

Thermodynamic states of a system with long-range dipole-dipole interactions between particles generally depend on the system's macroscopic shape. This dependence results from the boundary depolarization field modifying the sample's polarization, either electric or magnetic, that arises spontaneously or due to an external field. The influence of the sample shape on various properties of dipolar and magnetic systems was studied, for instance, in Refs. 1–3. It has become clear from the results of Refs. 4 and 5 that a dipolar system undergoing a phase transition into a state with spontaneous ferroelectric or ferromagnetic order is macroscopically inhomogeneous for all sample shapes, except for the needle.<sup>6</sup> This macroscopic inhomogeneity complicates investigations of the sample shape influence on the order-disorder phase transitions.<sup>7</sup>

The present work reports a theoretical study of the sample shape influence on the antiferroelectric (AFE) phase transitions in electro-dipolar systems in an external field. The macroscopic electronic polarization is generated in AFE systems only in the presence of the external field and, therefore, the ordered states of the model described below are spatially homogeneous for samples of all shapes. Since the macroscopic electric polarization is related via the depolarization factor to the sample shape, on the one hand, and to the AFE order parameter, on the other hand, the sample shape becomes yet another external parameter that influences the properties of the system. We show that in addition to such external parameters as temperature  $T$ , electric field  $E$ , and concentration of dipolar particles  $x$ , the macroscopic shape of a system determines its thermodynamic states and changes location and even the type of the phase transition. The results presented here for the electro-dipolar system are easily transferable to magnetodipolar systems.

The theoretical study reported here is based on the experimental investigation of polymer solutions of quasilinear dipolar chromophores (CP's).<sup>8–10</sup> These solutions merit attention for the following two main reasons. First, they form an excellent experimental realization of the model systems that are widely used in theory and simulation of liquid crystalline and electric properties of aggregates.<sup>7,11,12</sup> Second, the polymer solutions of dipolar CP's frozen in the presence of a strong poling field<sup>8–10,13,14</sup> possess a number of practically important nonlinear optical properties and find wide industrial applications. The quality and efficiency of such systems

is determined, to a large extent, by the maximum achievable macroscopic density of the dipole moment.

Experimental investigation of the nonlinear electro-optic coefficient<sup>8–10</sup> show that the density of the electric moment grows with increasing CP concentration, but later reaches a maximum and dramatically decays. This behavior has been explained by the growth of the AFE dipole-dipole interaction component.<sup>8–10</sup> References 15 and 16 develop an analytically solvable model that interprets the experimental observation by the phase transition from a paraelectric (PE) state to an AFE state. It has been shown that the dipole moment density and, as a result, the magnitude of the electro-optic coefficient are maximal at the point of phase transition between the disordered and ordered states. In correspondence to the experimental setup, References 15 and 16 considered the depolarization field of slab samples only, and noted that an explicit consideration of the slab boundary changes the location of the phase transition in the  $(E, x)$  plane. It was concluded, based on the results of Refs. 15 and 16 that the macroscopic shape of the sample could be accounted for in the investigation of AFE phase transitions in dipolar systems.

Here we present a systematic study of the effect of the change of the sample shape from oblate to prolate. First, we demonstrate how the location of the AFE phase transition in the  $(E, x)$  plane depends on the sample shape. Second, we observe that the type of the phase transition can change from first to second order, and that critical points of several kinds can appear and disappear as a result of the variation of the sample shape, while keeping the other external parameters fixed. It follows from the data below that the sample shape should be part of the phase transition coordinate set.

The model used here is similar to that of Refs. 15 and 16. It assumes that a system of quasilinear CP's at an experimentally relevant density exists in a nematic or smectic state. The state is formed due to the short-ranged excluded volume or Gay-Berne forces.<sup>17</sup> While formation of this state is not explicitly considered, it is important that the long axes of the quasilinear molecules are directed along the selected  $Z$  direction. The centers of mass of the molecules have a liquid-crystal position order, and the electric state of molecular dipoles is considered in the presence of this position order. The molecular dipoles are located in the molecular centers of mass, and are directed along the quasilinear molecular axes. The thermodynamic dipolar states arise as a result of com-

peting dipole-dipole and dipole-field interactions. The external electric field is directed along the selected  $Z$  axis. The shape of the sample is defined by the ellipsoid of revolution, and ranges from a plate to a needle. The orientations of the longest molecular axes stipulated by the spatial order suggests an Ising structure for the dipole-dipole Hamiltonian,

$$H = (\mu^2/2\varepsilon) \sum_{l \neq m} d(l,m) \sigma_l^z \sigma_m^z - (\mu E/\varepsilon) \sum_l \sigma_l^z \quad (1)$$

where  $\sigma_l^z = \pm 1$  is the Ising variable,  $\mu$  is the magnitude of the molecular dipole moment,  $\varepsilon$  is the polymer dielectric constant, and  $d(l,m) = [r_{lm}^2 - 3(r_{lm}^z)^2]/r_{lm}^5$ , where  $r_{lm}$  is the radius vectors between CP's  $l$  and  $m$ . For simplicity, the CP's are placed on a simple cubic lattice. We assume that the considered system of interacting dipoles exists as a function of the external parameters in either a PE or AFE state.<sup>15,16</sup> The AFE state has the following structure described in terms of two sublattices. CP's in chains along the  $Z$  axis belong to the same sublattice. CP's in adjacent chains belong to different sublattices. This type of state in dipolar Ising systems on a cubic lattice in the absence of the field was first considered in Ref. 18. The indices  $g$  and  $f$  enumerate CP's in the first and second sublattices, correspondingly. In the self-consistent two sublattice approximation, Hamiltonian (1) takes the form

$$\begin{aligned} H = & -(\mu^2 N/4\varepsilon)[(\sigma_1^2 + \sigma_2^2)A + 2\sigma_1\sigma_2B] \\ & + (\mu^2/\varepsilon) \left[ (\sigma_1 A + \sigma_2 B) \sum_g \sigma_g^z + (\sigma_2 A + \sigma_1 B) \sum_f \sigma_f^z \right] \\ & - (\mu E/\varepsilon) \left( \sum_g \sigma_g^z + \sum_f \sigma_f^z \right), \end{aligned} \quad (2)$$

Here  $N$  is the total number of CP's in the system.  $\sigma_1$  and  $\sigma_2$  are self-consistent parameters that in the equilibrium state give thermodynamically averaged dipole moments, i.e., polarizations of the first and second sublattices. The dipolar sums  $A$  and  $B$  are given by

$$A = \sum_{\delta_1} d(g, g + \delta_1) = \sum_{\delta_2} d(f, f + \delta_2), \quad B = \sum_{\delta_2} d(g, g + \delta_2),$$

where the summation indices  $\delta_1 \neq g$  and  $\delta_2 \neq f$  and run over the first and second sublattice CP's relative to CP's  $g$  and  $f$ . The dipolar sums are calculated by the well-known technique, e.g., Refs. 19 and 20, where each  $A$  and  $B$  is the sum of three terms. The first term comes from the summation over the CP's inside the Lorentz sphere. The other two terms are due to the electric charges accumulated on the external surface of the Lorentz sphere and on the internal surface of the sample. The dipolar sums inside the Lorentz sphere rapidly converge, and, similarly to Refs. 15 and 16, the nearest-neighbor approximation is used. The resulting expressions for  $A$  and  $B$  are

$$A + B = \pi(n - 1/3)/a^3, \quad A - B = -8/a^3,$$

where  $a$  is the cubic lattice constant, and  $n$  is the depolarization factor along the  $Z$  axis of the rotation ellipsoid. The values of  $n$  range from 0 for a needle to 1 for a plate. In a spherical sample,  $n = 1/3$ . The effective Hamiltonian [Eq. (2)] depends on the shape of the sample through its dependence on  $A$  and  $B$ .

Hamiltonian (2) produces the nonequilibrium thermodynamic potential of the system under study  $f(\sigma, l)$  that depends on the macroscopic polarization  $\sigma = (\sigma_1 + \sigma_2)/2$  and the AFE order parameter  $l = (\sigma_1 - \sigma_2)/2$ . At a constant temperature  $T$ , the thermodynamic potential normalized to  $NT/2$  is equal to

$$f(\sigma, l) = 2x \eta (l^2 - \alpha \sigma^2) - \ln(\cosh e_1) - \ln(\cosh e_2) - 2 \ln 2, \quad (3)$$

where  $x = 1/(a^3 10^{20})$  is the normalized number of particles in a unit volume,  $\eta = (4\mu^2 10^{20})/(\varepsilon T)$ ,  $e_{1,2} = e \pm bl - b\alpha\sigma$ , and  $e = (\mu E)/(\varepsilon T)$ . Note that the CP concentration  $x$  is contained in  $b = 2x\eta$ , while  $\alpha = \pi(n - 1/3)/2$  determines the shape dependence via the depolarization factor  $n$  and changes from  $-\pi/6$  to  $\pi/3$ . Setting the partial derivatives of potential (3) with respect to  $\sigma$  and  $l$  equal to 0, the following equations for the stationary values of  $\sigma$  and  $l$  are obtained:

$$2\sigma = \tanh e_1 + \tanh e_2, \quad 2l = \tanh e_1 - \tanh e_2. \quad (4)$$

The values of  $\sigma$  and  $l$  range in the interval  $0 \leq \sigma, l \leq 1$ . Solutions of Eqs. (4) with  $l = 0$  describe PE states, while solutions with  $l \neq 0$  describe AFE states.

*Paraelectric states.* With  $l = 0$ , the values of  $\sigma$  are found from the equation

$$\sigma = \tanh(e - \alpha b \sigma). \quad (5)$$

The region of stability of the PE states is given in the  $(E, x)$  plane by a line whose equation is found by first separating the PE solution of Eqs. (4) and then taking the  $l \rightarrow 0$  limit in the remaining solution. The resulting equation is

$$e = \ln(\sqrt{b} + \sqrt{b-1}) + \alpha \sqrt{b(b-1)}, \quad (6)$$

where the reduced electric field  $e$  is defined above, and  $b$  and  $\alpha$  are also defined above and are proportional to the CP concentration  $x$  and depolarization factor  $n$ , correspondingly. The PE state stability lines described by Eq. (6) are shown in Fig. 1 for different sample shapes. All lines start at the point  $(e_0 = 0, b_0 = 1)$ , independent of  $\alpha$ . The shape of the line, on the other hand, depends significantly on  $\alpha$ . For oblate samples with  $\alpha > 0$ , the electric field on the stability line grows with increasing CP concentration  $x$ . The growth is linear for large  $x$ . For the spherical case with  $\alpha = 0$ , the electric field grows as a logarithm of the concentration. The stability lines of prolate samples with  $\alpha < 0$  exhibit maxima at  $b = (1 - 1/\alpha)/2$  and terminate at  $e = 0$ . The CP concentration at the end of the line is determined by  $\exp[-\alpha \sqrt{b(b-1)}] = \sqrt{b} + \sqrt{b-1}$ . The PE state stability lines of prolate samples are qualitatively different from those of oblate samples. The PE states in prolate samples are unstable only within a finite bounded region on the  $(E, x)$  plane; see Fig. 1. The data are given for the following typical values of the parameters:  $\mu$

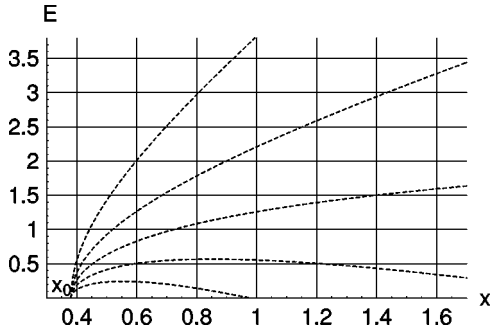


FIG. 1. Stability regions of the PE states. The lines from bottom to top correspond to depolarization factors of  $n=0, 0.15, \frac{1}{3}, 0.58,$  and 1. All lines start at the same point  $x_0$ , independent of the sample shape.

$=13D$ ,  $\varepsilon=1$ , and  $T=373$  K. The electric field  $E$  is given in characteristic units of  $100 \text{ V}/\mu\text{m}$ .<sup>8–10,15,16</sup>

*Antiferroelectric states.* Solutions to Eq. (4) with  $l \neq 0$  describe AFE states. Upon elimination of the PE solution, Eq. (4) can be conveniently expressed in the forms

$$e = ab\sigma + 0.5 \ln(\gamma + \sqrt{\gamma^2 - 1}), \quad (7)$$

$$\sigma = \sqrt{1 - 2l/\tanh(2bl) + l^2}, \quad \gamma = \sinh(2bl)/l - \cosh(2bl).$$

Equations (7) define the AFE state stability lines. The unusual shape of the PE stability line with  $\alpha < 0$  suggests that, in addition to the second-order phase transitions, the system under study can exhibit phase transitions of the first order. In this case, the lines separating the stability regions of the AFE states do not coincide with the stability lines for the PE states, and a region in  $(E, x)$  plane exists where the PE and AFE states are stable simultaneously. The equation describing the AFE stability lines is obtained by combining Eqs. (7) with their derivative with respect to  $l$ . After some transformations, the result is

$$2b(2b\alpha - \alpha + 1) = \frac{1}{l^2} \left( \frac{2bl}{\tanh(2bl)} - 1 \right) \left( \frac{2bl\alpha}{\tanh(2bl)} + 1 \right). \quad (8)$$

Given a value of  $l$  from the  $[0,1]$  interval, the AFE stability line is constructed by calculation of  $x$  from Eq. (8) and  $E$  from Eq. (7). Depending on the sample shape and other external parameters, the stability lines for the ordered states typically end in tricritical points ( $t$ ) located on the stability lines of the disordered states. The concentration at the tricritical point can be found from Eq. (8) in the limit of  $l \rightarrow 0$ :

$$b_t = [3(1 - \alpha)]/[2(1 - 2\alpha)]. \quad (9)$$

The electric field at the tricritical point is found by substituting  $b_t$  into Eq. (6).  $b_t$  reaches its minimum value of  $b_t \approx 1.116$  for needle-shaped samples with  $\alpha = -\pi/6$  and  $n = 0$ . As  $\alpha$  increases,  $b_t$  grows as well. For example, for sphere  $b_t = \frac{3}{2}$ . In the limit of  $\alpha \rightarrow \frac{1}{2}$  ( $n \rightarrow \frac{1}{3} + 1/\pi \approx 0.652$ ) the values of  $b_t \approx 3/[4(1 - 2\alpha)]$  and  $e_t \approx 3/[8(1 - 2\alpha)]$  become infinite. Thus, for oblate samples with  $\alpha \geq \frac{1}{2}$ , the tricritical

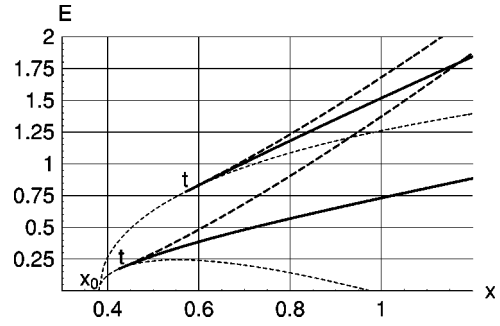


FIG. 2. Phase transitions in the needle-shaped sample with  $n = 0$  (bottom lines), and a spherical sample with  $n = \frac{1}{3}$  (top lines). Between points  $x_0$  and  $t$  the dashed lines describe the second order phase transition between the PE and AFE states. To the right of the tricritical points  $t$ , the system exhibits phase transitions of the first order (thick solid lines). The regions of stability of the PE and AFE states to the right of the tricritical points are given by long and short dashed lines, correspondingly.

point is absent; therefore, the AFE stability lines in the first-order phase transition region of the phase diagram do not terminate at the PE stability lines.

Numerical investigation of the AFE stability lines for different  $\alpha$  shows lines of two types. According to Eqs. (7) and (8) with  $l$  changing from 0 to 1, the concentration and electric field both increase along the lines of the first type, as illustrated by the bold dashed lines in Fig. 2. This behavior is characteristic of the needle and spherical samples. Unusual beak-shaped lines of the second type appear for the samples with  $\alpha > \alpha_0$ , the value of  $\alpha_0$  to be determined below. Lines of the second type are illustrated by bold dashes in Fig. 3. Prior to the normal increase with increasing  $l$ , lines of this type decrease toward the apex of the beak. The apex is the critical point of the first-order phase transition. The AFE states within the narrow concentration interval inside the beak compete not only with the PE states, but also with another set of AFE states characterized by different values of  $\sigma$  and  $l$ . The coordinates of the critical point can be found by combining Eq. (8) with its derivative with respect to  $l$ :

$$4(2b\alpha + 1 - \alpha)(2 - y_l^{(1)}l)/l^2 - 2b\alpha y_l^{(1)}y/l^3 = 0, \quad (10)$$

where  $y = [2bl/\tanh(2bl) - 1]/b$  and  $y_l^{(1)}$  is the derivative of  $y$  with respect to  $l$ . As  $l$  approaches 0, the coordinates of the critical point [Eq. (10)] approach the coordinates of the tricritical point [Eq. (9)]. This condition gives  $\alpha_0 = \frac{1}{4}$ . Therefore, beak-shaped AFE stability lines with the critical points inside the ordered phase exist only in the samples with  $\alpha > \frac{1}{4}$ . A similar behavior was observed in antiferromagnetics with a single ion anisotropy.<sup>21,22</sup> As follows from an analysis of Eqs. (9) and (10), the existence of the critical point puts an upper bound on  $\alpha$ , which is  $\alpha = 1$ , corresponding to  $n = 1/3 + 2/\pi \approx 0.97$ . Approaching the upper bound, the coordinates of the critical point evolve as  $b_c, e_c \sim 2/(1 - \alpha)$ , and diverge to infinity. Thus the critical point exists only in samples with  $1 > \alpha > \frac{1}{4}$ . In the narrow interval of  $\pi/3 \geq \alpha \geq 1$  only second-order phase transitions are possible. In particular, in flat, plate-shaped samples that are typical in the experiments,<sup>8–10</sup>

only second-order phase transitions are possible over the whole parameter range, as illustrated in Fig. 1 by the AFE stability line for  $n = 1$ .

Phase transitions of the first order occur on the lines of thermodynamic equilibrium between the two phases. The equilibrium lines are obtained by equating the thermodynamic potentials [Eq. (3)] corresponding to PE and AFE states

$$f(\sigma_p, 0) = f(\sigma_a, l), \quad (11)$$

where  $\sigma_p$  obeys Eq. (5) and  $\sigma_a$ ,  $l$  obey Eq. (7), as shown in Fig. 2 by solid lines. For clarity, only cases without the critical points are illustrated. In the presence of critical points, two closely spaced phase transition lines coexist near the beak in the  $(E, x)$  plane. For instance, if in Fig. 3 the concentration is kept constant at  $x = 1.2$  and the strength of the electric field is increased, an ordered state that exists at low fields will transform into another ordered state after crossing the first-order phase-transition line. Then the second ordered state will turn into a PE state by crossing the line of the second-order phase transitions.

In summary, we have shown that the macroscopic shape of the sample strongly influences the phase transitions in the Ising dipolar AFE that is subjected to an external electric field. Substantial quantitative and qualitative changes in the phase diagram occur as the shape of the sample changes from a needle with a depolarization factor  $n = 0$  to a plate with  $n = 1$ . Critical and tricritical special points appear on the phase diagram depending on the sample shape. Only within a small range of  $1 \geq n \geq 1/3 + 2/\pi$  does the phase diagram con-

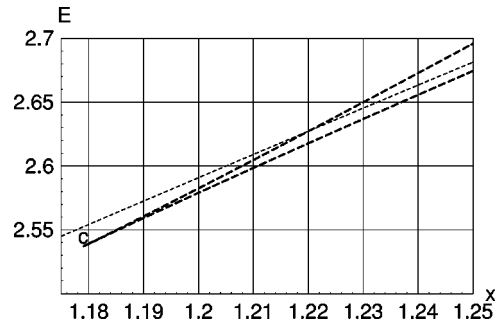


FIG. 3. The beaklike fragment of the stability regions of the AFE (thick dashed line) and PE (thin dashed line) states for the oblate ellipsoid with the depolarization factor  $n = 0.58$ . The first-order phase-transition critical point is denoted by  $c$ . The tricritical point with coordinates  $x = 1.555$  and  $E = 3.21$  lies outside the scale of the figure. The phase equilibrium line (the thick solid line in Fig. 2) is omitted for clarity.

tain a single second-order phase transition line. For other values of  $n$  various combinations of the first- and second-order phase transitions are present. The range of  $n$  responsible for the coexistence of the tricritical and critical points is determined. The  $T$ ,  $\mu$ , and  $\varepsilon$  parameters have been held fixed in this study, but can be used to shift the special points to an experimentally convenient region.

Financial support of NSF, Award No. 0994012 and University of Washington Royalty Research Fund is gratefully acknowledged.

\*Corresponding author. Email address: prezhd@u.washington.edu

- <sup>1</sup>B. Groh and S. Dietrich, Phys. Rev. Lett. **72**, 2422 (1994).
- <sup>2</sup>T. Buishvili, R. Khomeriki, and L. Tkeshelashvili, Phys. Rev. B **64**, 012 405 (2001).
- <sup>3</sup>S. Kolesnik, T. Skoskiewicz, J. Igalson, and Z. Korczak, Phys. Rev. B **45**, 10 158 (1992).
- <sup>4</sup>B. Groh and S. Dietrich, Phys. Rev. Lett. **79**, 749 (1997).
- <sup>5</sup>S. Banerjee, R. B. Griffiths, and M. Widow, J. Stat. Phys. **93**, 109 (1998).
- <sup>6</sup>P. I. C. Teixeira, M. A. Osipov, and M. M. Telo da Gama, Phys. Rev. E **57**, 1752 (1998).
- <sup>7</sup>B. Groh and S. Dietrich, Phys. Rev. E **53**, 2509 (1996).
- <sup>8</sup>Y. Shi, C. Zhang, H. Zhang, J. H. Bechtel, L. R. Dalton, B. H. Robinson, and W. H. Steier, Science **288**, 119 (2000).
- <sup>9</sup>B. H. Robinson, L. P. Dalton, A. W. Harper, A. Ren, F. Wang, C. Zhang, G. Todorova, M. Lee, R. Aniszfeld, S. Garner, A. Chen, W. H. Steier, S. Houbrecht, A. Persoons, I. Ledoux, J. Zyss, and A. K. Y. Jen, Chem. Phys. **245**, 35 (1999).
- <sup>10</sup>A. K. Y. Jen, Y. Q. Liu, L. X. Zheng, S. Liu, K. Y. Drost, Y. Zhang, and L. R. Dalton, Adv. Mater. **11**, 452 (1999).
- <sup>11</sup>S. C. McGrother and G. Jackson, Phys. Rev. Lett. **76**, 4183 (1996).

- <sup>12</sup>P. J. Camp, J. C. Shelley, and G. N. Patey, Phys. Rev. Lett. **84**, 115 (2000).
- <sup>13</sup>P. M. Lundquist, S. Yizchaik, T. J. Marks, G. K. Wong, S. Di Bella, R. Cohen, and G. Berkovic, Phys. Rev. B **55**, 14 055 (1997).
- <sup>14</sup>M. Yu. Balakina, J. Li, V. M. Geskin, S. R. Marder, and J. L. Bredas, J. Chem. Phys. **113**, 9598 (2000).
- <sup>15</sup>Y. V. Pereverzev and O. V. Prezhdo, Phys. Rev. E **62**, 8324 (2000).
- <sup>16</sup>Y. V. Pereverzev, O. V. Prezhdo, and L. P. Dalton, Chem. Phys. Lett. **240**, 328 (2001).
- <sup>17</sup>J. G. Gay and B. J. Berne, J. Chem. Phys. **74**, 3316 (1981).
- <sup>18</sup>J. M. Luttinger and L. Tisza, Phys. Rev. **72**, 257 (1947).
- <sup>19</sup>A. I. Akhiezer, V. G. Baryakhtar, and S. V. Peletminskii, *Spin Waves* (North-Holland, Amsterdam, 1968).
- <sup>20</sup>D. C. Mattis, *The Theory of Magnetism* (Harper & Row, New York, 1965).
- <sup>21</sup>V. G. Bar'Yakhtar, I. M. Vitebskii, and D. A. Yablonskii, Fiz. Tverd. Tela (Leningrad) **19**, 21 (1997) [Sov. Phys. Solid State **19**, 1249 (1977)].
- <sup>22</sup>A. A. Loginov and Y. V. Pereverzev, Fiz. Nizk. Temp. **24**, 867 (1998) [Low Temp. Phys. **24**, 652 (1998)].